

## ULTRASTRUCTURAL TOPOCHEMISTRY OF CELL WALL POLYMERS IN *POPULUS NIGRA* BY TRANSMISSION ELECTRON MICROSCOPY AND RAMAN IMAGING

Jianfeng Ma,<sup>a</sup> Zhiheng Zhang,<sup>a</sup> Guihua Yang,<sup>b</sup> Jianzhen Mao,<sup>a</sup> and Feng Xu<sup>a,\*</sup>

The topochemical distribution of lignin and cellulose in individual cell wall layers of *Populus nigra* stem was determined by transmission electron microscopy (TEM) and confocal Raman microscopy. TEM images exhibited the fiber wall as being typically differentiated into three layers: middle lamella (ML), primary wall (P), and secondary wall (S<sub>1</sub>, S<sub>2</sub>, and S<sub>3</sub>). Higher magnification views showed the S<sub>2</sub> layer to be differentiated into electron lucent and dense areas in the radial direction. In situ Raman images calculated by integrating over the intensity of characteristic spectral bands enabled visualization of the spatial variation in lignin and cellulose. Raman images acquired by integrating over the spectral band at 1605 cm<sup>-1</sup> suggested that higher lignin content was visualized in the cell corner (CC), the compound middle lamella (CML), and the secondary wall of ray parenchyma. Cellulose distribution followed by taking the band regions around 2897 cm<sup>-1</sup> into account showed the opposite pattern, with the highest content in fiber secondary wall. The SEM-EDXA provided semi-quantitative results, showing that the lignin content ratio in various cell wall layers was 1.4 (CC):1.1(CML):1(S<sub>2</sub>).

*Keywords:* *Populus nigra*; Cell wall polymers; TEM imaging; Raman imaging

*Contact information:* a: Institute of Biomass Chemistry and Technology, Beijing Forestry University, Beijing, China, 100083; b: Key Lab of Paper Science and Technology of Ministry of Education of China, Shandong Polytechnic University, Ji'nan, China, 250353; \* Corresponding author: xfx315@163.com

### INTRODUCTION

Research into lignocellulosic biomass has experienced dramatic growth in recent years due to its abundance in nature and renewable character. The aim of economically feasible biomass processing is to achieve a complete utilization of various biomass components. Under ideal conditions, lignocellulosic biomass can be broken down by a series of chemical, enzymatic, and microbiological processes into ethanol or other biofuel resources. Lignocellulosic biofuel production involves collection of biomass, deconstruction of cell wall carbohydrate polymers into component sugars, and conversion of the sugars to biofuels (Rubin 2008). The recalcitrance of walls to saccharification, however, poses a major impediment for conversion of lignocellulosic biomass to biofuels (Himmel et al. 2007). Plant cell walls have evolved complex structural and chemical mechanisms for resisting assault on its structural sugars from microbes and other decay organisms. In lignified tissue, between the ordered cellulose fibrils, the lignin-hemicellulose matrix is probably highly organized, with the glucomannan closely associated with the cellulose. Meanwhile, the lignin aromatic rings are preferentially oriented in the transverse direction and along the cellulose fibrils (Åkerholm and Salmén 2003). The detailed

structure of plant cell wall, however, remains to be fully elucidated. Yet such a detailed knowledge is required to understand the specific chemical and physical obstacles to breakdown.

Cellulose, which is composed of chains of approximately  $8 \times 10^3$  D-glucopyranose residues linked together by  $\beta$ 1-4 glycosidic bonds, is abundant in plant cell walls. Hemicelluloses, the second most abundant constituent of lignocellulosic biomass, is not a chemically well defined compound but rather a family of polysaccharides, composed of different 5- and 6-carbon monosaccharide units, that links cellulose microfibrils into fibers and cross-links with lignin, creating a complex network of bonds that provide structural strength. Both cellulose and hemicelluloses can be hydrolyzed to provide fermentable sugars for bioethanol production. Lignin is a complex and irregular polyphenylpropanoid heteropolymer present in the cell walls of vascular plants. In plant anatomy, lignin can be considered as the cellular glue, providing the plant tissue and the individual fibers with compressive strength and the cell wall stiffness (Boerjan et al. 2003). In biomass conversions, the presence of lignin limits the accessibility of plant cell wall polysaccharides to chemical, enzymatic, and microbial digestion. The recalcitrance of cell walls originates not only from the composition of the cell wall polymers, but also from fine details of their macromolecular structure and conformation, and on their highly ordered architecture at scales from a few nanometers to several microns. Much of this fine detail is lost when cell-wall polymers are fractionated or solubilized to be examined by the classical chemical techniques. Therefore, spectroscopic approaches play an important role to examine plant cell walls in their native state.

To generate chemical images in situ from biological tissues brings a wealth of information, as it is not solely a chemical analysis of the sample, but of the intact tissue in context with the anatomy and spatial distribution within the sample. Raman spectroscopy, based on the discrete vibrational transitions that take place in the ground electronic state of molecules, can be used for probing structure, dynamics and function of biomolecules (Gierlinger and Schwanninger 2007). Analogously to spectra obtained with other vibrational techniques, Raman spectra of biological molecules contain numerous bands representing molecular normal modes of vibration that serve as sensitive and selective fingerprints of their structure, composition, interactions, and dynamics. A number of organic compounds and functional groups can be identified by their unique spectral patterns, and the intensity of the bands may be used for the calculation of the relative content in the sampled entity. By combining this technique with microscopy, molecular information can be obtained with high spatial resolution, samples of microscopic size can be analyzed directly wet or dry, and in many cases this can be done non-destructively. For in situ compositional and structural analysis of lignocellulosic materials whose microstructure is composed of morphologically distinct regions, Raman microscopy is an effective technique.

Here, the transmission electron microscopy (TEM) was used to investigate the ultrastructural characteristics of *Populus nigra* fiber cell wall. The confocal Raman microscopy was employed to acquire spectra maps and chemical images of *Populus nigra* stem cross-sections. The SEM-EDXA technique was used to reveal the variation in lignin content semi-quantitatively. The principal results revealed the differences in lignin and cellulose content together with the chemical composition in the cell wall layers.

## EXPERIMENTAL

### Material

A 5-year-old *Populus nigra* tree was supplied by the arboretum of Northwest Agricultural and Forest University, China. Specimens were taken from the sapwood at a tree height of 1.3 m and dissected into small blocks. These blocks were preserved in ethanol and glycerin (1:1 v/v) until used.

### Transmission Electron Microscopy (TEM) Analysis

Blocks taken from *Populus nigra* sapwood were cut into small strips ( $1 \times 1 \times 2 \text{ mm}^3$ ). These samples were dehydrated in acetone and embedded in Spurr's low viscosity resin. Ultrathin sections (90 nm) were cut with a diamond knife on a Leica Ultramicrotome (EM-UC6). The sections were stained with 1% w/v  $\text{KMnO}_4$  (prepared in 0.1% w/v sodium citrate) for 3 minutes at room temperature. The micromorphological features of the various layers of latewood fiber and vessel were examined with a JEM-1230 transmission electron microscope at 80 kV (Singh et al. 2002).

### Scanning Electron Microscopy with Energy Dispersive X-ray Analysis (SEM-EDXA)

Transversely cut sections of 20  $\mu\text{m}$  thickness obtained by using a sliding microtome were extracted with a mixture of benzene-ethanol (2:1, v/v) for 24 h. Subsequently, they were reacted with 1%  $\text{KMnO}_4$  for 5 min at room temperature and air-dried. After coating with a 10-nm thick gold film by evaporation, lignin distribution was measured semi-quantitatively by Hitachi S-4300 SEM-EDXA. The accelerating voltage and probe current used were 20 kV and 80  $\mu\text{A}$ , respectively. The point analysis (100 seconds) of Mn-K X-rays was performed with a Horiba Si (Li) energy-dispersive spectrometer.

### Confocal Raman Microscopy

For Raman microscopy the cross sections were put on a glass slide with a drop of water, covered by a coverslip (0.17 mm thickness) and sealed with nail-polish to avoid evaporation. Raman spectra were acquired with a LabRam Xplora confocal Raman microscope (Horiba Jobin Yvon) equipped with a confocal microscope (Olympus BX51), a motorized x, y stage, and a high numerical aperture (NA) microscope objective from Olympus (MPlan 100 $\times$  objective, NA=0.90). A linear-polarized 633-nm laser excitation was focused with a diffraction-limited spot size ( $1.22\lambda/\text{NA}$ ). The laser power on the sample was approximately 8 mW. For mapping, 0.5  $\mu\text{m}$  steps were chosen, and every pixel corresponds to one scan. The spectrum from each location was obtained by averaging 2-s cycles. Confocal aperture was set at 400  $\mu\text{m}$  for all experiments. The reported depth resolution for the 400  $\mu\text{m}$  confocal hole, based on the silicon (standard) phonon band at  $520 \text{ cm}^{-1}$ , was 2  $\mu\text{m}$ . The lateral resolution of the confocal Raman microscope was 1  $\mu\text{m}$ , which was bigger than the theoretical limit ( $0.61\lambda/\text{NA} \approx 430 \text{ nm}$ ). The software (Labspec) was used for measurement setup and image processing. The spectra were baseline corrected using the Savitsky-Golay algorithm for spectroscopic analysis. The overview

chemical images enabled us to separate cell wall layers and to mark defined distinct cell wall areas to calculate average spectra from these areas of interest (Agarwal 2006).

The absolute Raman signal of a solid sample with a given composition varies with surface characteristics such as roughness, reflectivity, and the direction of the surface normal (Kurti et al. 2005). For samples such as the wood surfaces used in this study, semi-quantitative determinations require a normalization procedure. In this work, the analytical peak area was normalized by dividing by the area of the silicon signals at  $520.7\text{ cm}^{-1}$ . In that way, the silicon served as an external standard for the wood section. Various intensity ratios were calculated using the characteristic peaks of lignin, cellulose and Si by means of curve fitting. Raman intensity ratios ( $I_{\text{Lignin}}/I_{\text{Si}}$  and  $I_{\text{Cellulose}}/I_{\text{Si}}$ ) were used as spectral parameters characterizing changes of lignin and cellulose concentration.

## RESULTS AND DISCUSSION

### Ultrastructure of Fiber Cell Wall

The transmission electron micrographs revealed the ultrastructural features of fiber cell walls. Figure 1 shows the transverse section of *Populus nigra* fiber cell walls composed of intercellular layers: the middle lamella (ML), the primary wall (P), and the secondary wall (S<sub>1</sub>, S<sub>2</sub> and S<sub>3</sub>).

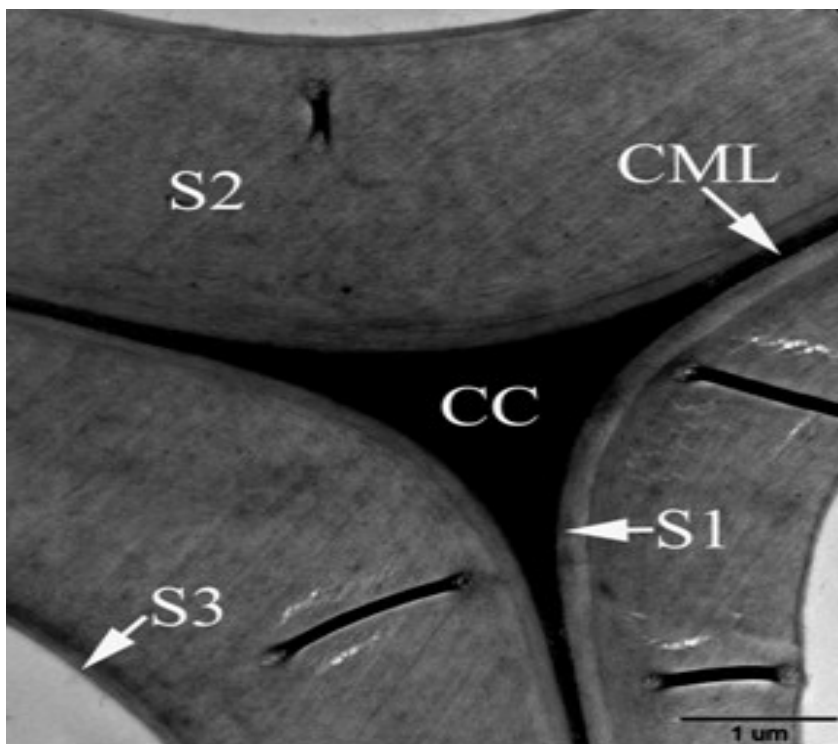


**Fig. 1.** TEM micrograph showing the ultrastructure of adjoining fibers, taken at 80 kV. The specimen was stained with 1% w/v  $\text{KMnO}_4$  (prepared in 0.1 % w/v sodium citrate). CC: cell corner, CML: compound middle lamella, S<sub>1</sub>: outer layer of secondary wall, S<sub>2</sub>: middle layer of secondary wall, S<sub>3</sub>: inner layer of secondary wall

The differences between the wall layers can be easily identified by the thickness of the cell wall. The primary cell wall (P) is a thin boundary at the outer layer of the cell. Boundaries between primary wall layer and middle lamella could not be exactly determined, as the primary wall is extremely thin (70-90 nm). Therefore, both the middle lamella (ML) and the contiguous primary wall (P) are termed compound middle lamella (CML), which is approximately 0.14  $\mu\text{m}$  in width. The secondary wall is a thick layer located inside the primary wall in the inner part of the cell, consisting of an outer layer ( $S_1$ ), a middle layer ( $S_2$ ), and an inner layer ( $S_3$ ). The  $S_1$  layer in *Populus nigra* fiber is well-defined and could be distinguished from the adjoining  $S_2$  layer based on variation of staining intensity. Obviously, the thickness of the  $S_1$  layer (0.21-0.27  $\mu\text{m}$ ) is highly variable within cells, being widest in cell corner regions. The  $S_2$  layer accounts for the largest proportion of the entire fiber wall. Random measurements were taken on high magnification TEM micrographs, and the thickness of the  $S_2$  layer in fibers was found to be in the range of 1.69 to 2.45  $\mu\text{m}$ . Also, measurement of the thickness of the  $S_3$  layer taken from a large number of high magnification TEM micrographs showed the thickness of this layer to vary from 0.05  $\mu\text{m}$  to 0.11  $\mu\text{m}$ . The irregular thickness might be better suited than uniform thickness to relieve the axial compression force on the fiber walls.

### Lignin Distribution by TEM

Transmission electron microscopy has proven to be an effective tool for determining various aspects of wood cell wall structure. Since the 1990s, the  $\text{KMnO}_4$  technique has been used in order to learn more about the lignification process during cell differentiation. The lignin-staining ability of  $\text{KMnO}_4$  makes it a very suitable technique for TEM. In this case, the lignin molecule is oxidized by  $\text{KMnO}_4$ . The permanganate anion is reduced to manganese dioxide, which then precipitates as electron-opaque sediments indicating the site of reaction (Donalson et al. 2001).

In all lignocellulosic fibers, cell wall layers contain cellulose, hemicelluloses, and lignin in varying amounts. Cellulose attains its highest content in the  $S_2$  layer, and lignin is most concentrated in the middle lamella, which, in principle, is free of cellulose (Saar et al. 2010; Schmidt et al. 2010). TEM observations provided further details of lignification. It is well known that the distinctive feature of the fiber walls is that lignin deposit is not uniform, and the CC generally is more highly lignified than other cell wall layers. In the present study, different cell wall layers could be clearly identified in TEM micrographs because of the electron-opaque sediments in those regions. The CC and the CML showed darker staining compared to the adjacent secondary wall layer. The electron-opaque particles of the CML are interpreted to be deposits of lignin due to the electron opacity of manganese dioxide, which complexes with lignin (Bland et al. 1971; Maurer and Fengel 1991). Within the CML, the inhomogeneity in lignin distribution is apparent, as judged by the presence of discrete electron-lucent regions in some parts of the middle lamella, being the most prominent in cell corners. Meanwhile the electron density decreased from the CC to P. The consecutive  $S_1$  layer appears more electron-lucent than other regions of the secondary wall, which means that this layer has far lower lignin content (Fig. 2a). The transition between  $S_1$  and  $S_2$  is characterized by a change in microfibril direction and also by an increase in lignin content. The gap between cellulose microfibrils is filled with a thin layer of lignin-hemicelluloses complex (Terashima

2000). The  $S_3$  layer is distinctly denser than inner parts of the  $S_2$  layer and slight undulation in places (Fig. 1).

Observations over a range of TEM magnifications showed that the micro-morphological appearance of the  $S_2$  layer with respect to lignin distribution varied depending upon the resolution at which the observations were made. Lower magnification images showed gross differences between fibers with regard to the distribution of lignin in the  $S_2$  layer, but the pattern of nano-level lignin distribution appeared to be similar. From the lower magnification views shown in Fig. 2b, the  $S_2$  layer appears to be denser in some regions than in others. The outer (near compound middle lamella) and inner (near cell lumen) parts of the  $S_2$  layer appear more electron-dense than the middle part. Variability in density is also apparent within both the outer and inner denser parts of this layer. In the inner  $S_2$ , the density appears to be the greatest in cell corner areas. In the outer  $S_2$ , the pattern of variability in the density is less consistent. The other striking feature of the fiber walls in Fig. 2c is that the  $S_2$  layer appears to have fine striations in radial directions and to be a mosaic of electron-dense and electron-lucent regions. The striations are most pronounced in the mid part of the  $S_2$  layer, where the wall appears to be lowest in density. The radially oriented dense and lucent regions are prominent, presenting a sinuous pattern. The non-linear pattern of the lucent regions (and correspondingly of the dense regions) across the thickness of the  $S_2$  layer can be explained by the previous observations (Kataoka et al. 1992), showing microfibril angles to change in successive waves of deposition, leaving spaces between stripes (bundles). The sinuous appearance of the lucent regions suggested that microfibril bundles are not likely to be linear in their distribution across the width of the  $S_2$  layer but may be arranged randomly. Previously, Singh and Daniel (2001) have reported that the  $S_2$  layer in the tracheids walls of *Picea abies* wood showed fine striations in both radial and tangential directions. The concentrically oriented dense and lucent regions were nearly straight with only slight sinuosity.

Additionally, the TEM image represented the variability in lignin content among cells. From Fig. 2d, the lignification level of the vessel secondary wall is higher than that of the fiber, which was in accordance with previous studies (Takabe et al. 1986; Yoshinaga et al. 1992). Generally, the vessel walls must withstand larger compressive forces resulting from the transpiration stream in plants, and hence a higher lignification level of the cell wall would be expected to increase the compression strength of the vessel and reduced its susceptibility to collapse (Donaldson 2001).

### Lignin Distribution by SEM-EDXA

SEM-EDXA has the merits of both keeping good resolution and measuring the deposition of lignin specifically. In this study, point scans were used for the semi-quantitative assay of lignin distribution.  $KMnO_4$  has been widely used to contrast lignin in the electron microscopic studies of plant and wood cells. This stain appears to be specific to lignin, although there are suggestions that it may also stain some hemicelluloses, but not cellulose (Saka 1982). Point analyses obtained from the cell corner, compound middle lamella, and secondary wall of fibers are shown in Table 1. A relative ratio of the measured Mn-K X-ray intensities directly provides element Mn content ratio, from which the ratio of lignin content in different morphological regions can be

estimated. In fiber cell walls, greater percent content of element Mn in CC (52.7) can be detected relative to that in CML (42.4) and S<sub>2</sub> layer (38.2).

When the Mn content in the S<sub>2</sub> layer of fiber walls is assumed to be 1, the content ratio in CC: CML: S<sub>2</sub> is 1.4:1.1:1. Therefore, we can assume that the lignin content ratio of fiber cell walls in CC, CML and S<sub>2</sub> is 1.4:1.1:1.

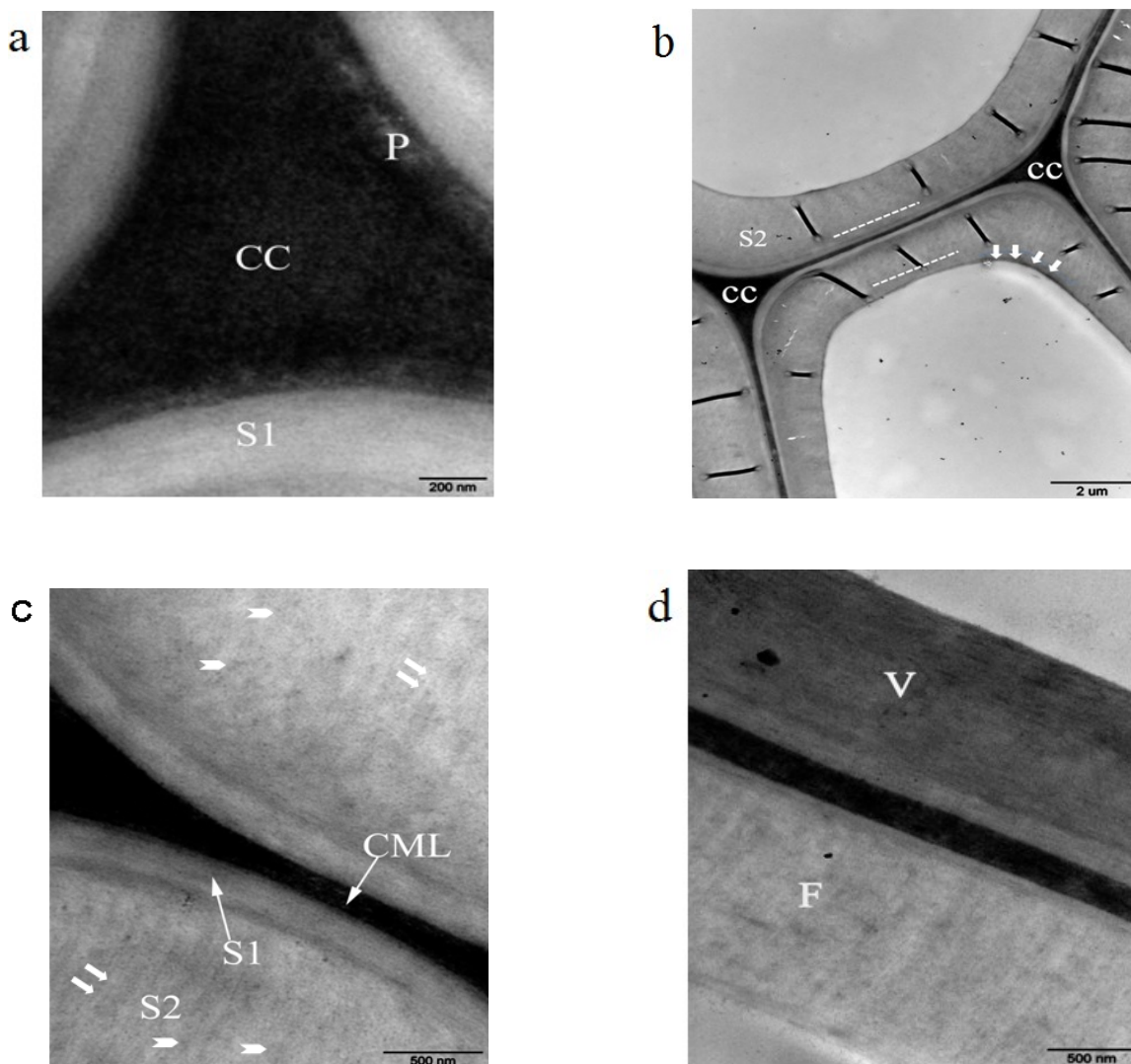


**Fig. 2.** TEM images showing the inhomogeneous distribution of lignin, taken at 80 kV. (a) The CC and P showed higher electron density than the adjacent S<sub>1</sub>; (b) The outer and inner parts of the S<sub>2</sub> layer appear more electron dense (stipplings) than the mid part, the density being particularly pronounced in the curved region of the wall (arrows); (c) The lignin distribution in the S<sub>2</sub> layer is distinctly inhomogeneous, with the wall appearing to be a mosaic of electron-dense (arrowheads) and electron-lucent (arrows) regions. The lucent regions have a pattern of sinuous features along the radial directions; (d) The dark staining of the vessel indicated that it is highly lignified, V: vessel, F: fiber

**Table 1.** The Content (%) of Element Mn in Morphologically Distinct Regions of Fiber Determined by the SEM-EDXA

Analytic points	CC	CML	S <sub>2</sub>
1	50.4	40.8	33.3
2	54.2	43.6	37.4
3	51.4	42.2	38.4
4	56.6	40.4	40.2
5	52.5	41.4	38.2
6	53.0	43.3	38.6
7	53.7	41.6	38.6
8	51.9	44.7	39.8
9	52.5	43.7	36.9
10	51.2	42.7	40.1
<b>Average</b>	<b>52.7</b>	<b>42.4</b>	<b>38.2</b>
Standard deviation	1.78	1.39	2.02

### Raman Spectra from Fiber Secondary Wall

Average spectra were calculated for the different cell wall layers (S<sub>2</sub>, CC and CML) by marking the distinct areas on the chemical images (Fig. 3). Raman band assignments for the secondary wall of *Populus nigra* fiber, shown in Table 2, are based on analogy with previous reports (Wiley and Atalla 1987; Agarwal and Ralph 1997; Edwards et al. 1997; Agarwal 1999; Saariaho et al. 2003; Rösch et al. 2004; Agarwal and Ralph 2008; Schmidt et al. 2009). The Raman bands are attributable primarily to the major wood polymers (cellulose and lignin) found in *Populus nigra*.

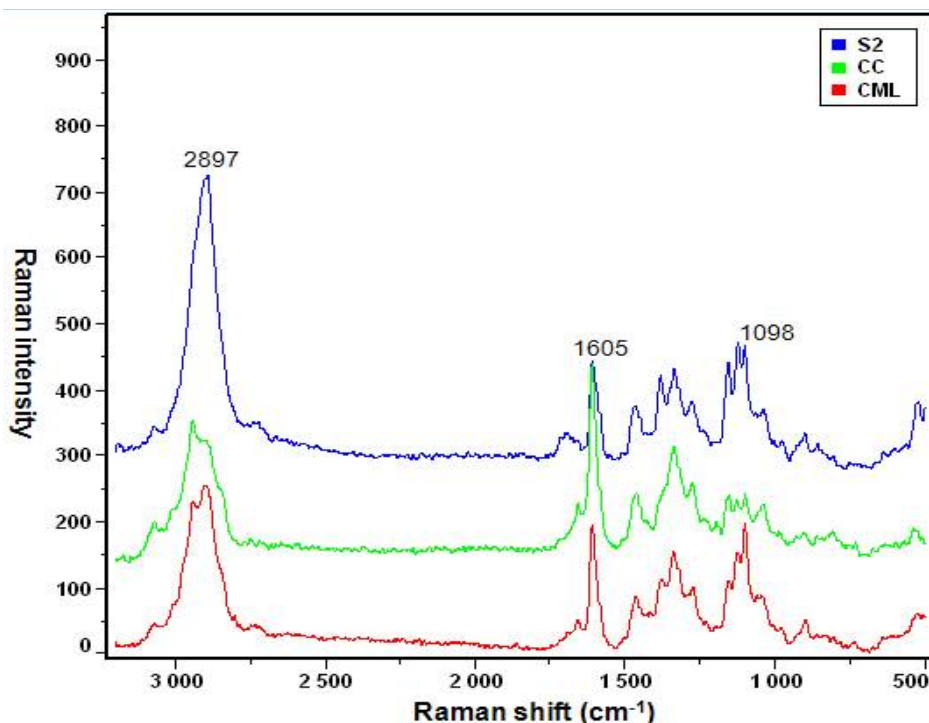
It is noted that in the region between 1700 cm<sup>-1</sup> and 1600 cm<sup>-1</sup> the vastly dominant spectral contribution stems from lignin. The 1605 cm<sup>-1</sup> band due to aryl ring stretching is a more general lignin marker. The other main lignin feature was detected at 1650 cm<sup>-1</sup>, due to the coniferaldehyde and sinapaldehyde together with coniferyl and sinapyl alcohol units. The characteristic cellulose vibrations can be seen in the region from 1500 to 1000 cm<sup>-1</sup>. At 1121 cm<sup>-1</sup> the symmetric stretching vibration of the C-O-C glucosidic linkage in combination with the C-O-C ring breathing vibration is observed, whereas the asymmetric stretching vibration of the C-O-C glycosidic linkage is located at 1098 cm<sup>-1</sup>. The band in the C-H stretching region at 2897 cm<sup>-1</sup> is also assigned to cellulose.

**Table 2.** The Raman Bands ( $\text{cm}^{-1}$ ) in the Average Spectra of the  $S_2$  Layer of *Populus Nigra* Fiber

Frequency ( $\text{cm}^{-1}$ )	Component	Assignment
2945	Lignin, Glucomannan	C-H stretching in $\text{OCH}_3$ asymmetric
2897	Cellulose	C-H and C-H <sub>2</sub> stretching
1650	Lignin	Ring conjugated C=C stretching of coniferyl and sinapyl alcohol; C=O stretching of coniferaldehyde and sinapaldehyde
1605	Lignin	Aryl ring stretching symmetric.
1504	Lignin	Aryl ring stretching asymmetric
1464	Lignin and Cellulose	HCH and HOC bending
1438	Lignin	O-CH <sub>3</sub> deformation; CH <sub>2</sub> scissoring; guaiacyl ring vibration
1378	Cellulose	HCC, HCO and HOC bending
1333	Cellulose	HCH and HCO bending
1277	Lignin	Aryl-O of aryl OH and aryl O-CH <sub>3</sub> ; guaiacyl ring (with C=O group) mode
1152	Cellulose	Heavy atom (CC and CO) stretching. plus HCC and HCO bending
1121	Cellulose, Xyl, and GlcMan	Heavy atom (CC and CO) stretching
1098	Cellulose, Xyl, and GlcMan	Heavy atom (CC and CO) stretching
1042	Xylan	Heavy atom (CC and CO) stretching
998	Cellulose	
902	Cellulose	Heavy atom (CC and CO) stretching
521	Cellulose	some heavy atom stretching

Xyl:Xylan

GlcMan:Glucomannan

**Fig. 3.** Average Raman spectra acquired from  $S_2$ , CC and CML, 3200-500  $\text{cm}^{-1}$

### Raman Imaging of Lignin Distribution

Raman microprobe studies on wood brought important insights into the macromolecular organization and compositional variability of the cell wall. Fibers and fibers adjacent to ray parenchyma on a cross-section were investigated. Chemical images were calculated by integrating over defined bands observed in the Raman spectra. The results showed mainly signals of two macromolecules, lignin and cellulose.

To obtain chemical images, position-resolved microspectroscopic measurements were performed, acquiring two dimensional spectral maps. The basic morphology of the measured cell walls becomes apparent in the chemical images based on the composite aromatic C=C stretching bands, integrating the intensity over the range from 1712 to 1519  $\text{cm}^{-1}$ . The main signals of lignin include 1605  $\text{cm}^{-1}$  (the aromatic ring stretching vibration) and 1650  $\text{cm}^{-1}$  (coniferaldehyde and sinapaldehyde together with coniferyl and sinapyl alcohol). The 1650  $\text{cm}^{-1}$  contribution was included not only because it is a lignin feature but also because of its partial overlap with the band at 1605  $\text{cm}^{-1}$ .

Lignin signal intensity within morphologically distinct regions of fiber is inhomogeneous (Fig. 4a). High lignin signal intensity is observed in the CC and somewhat less, in the CML. The lower, yet not insubstantial, amounts of lignin are observed within the secondary walls. However, there is variability of the lignin signal intensity and some secondary walls, namely of rays, are strongly lignified (Fig. 4b). The result is similar to previous studies of lignin distribution pattern (Xu et al. 2006; Abdul Khalil et al. 2010), and is in accordance with the hypothesis that lignification occurs initially in the cell corners and then cell walls (from the  $S_1$  to the  $S_3$ ). For any given morphological region the band intensity was location specific. Therefore, for a particular region, band intensities were compared to get a sense of the range of variation in lignin content. Such comparisons indicated significant variation. For an average fiber  $S_2$  lignin content of 82 intensity units expressed as a ratio to the highest and lowest CC lignin content of intensity units, the ratio was found to be 2.54 and 1.23 respectively. As far as what else could be behind the variation in lignin band intensity in addition to composition, the variation may be a reflection of lignin orientation (Cao et al. 2006). Further investigations specially aimed at this aspect of the findings are needed in order to reveal the extent to which variation in intensity can be interpreted in terms of orientation and concentration effects.

In the C-H stretching region (2840-2975  $\text{cm}^{-1}$ ) of the CC spectrum, the peak at 2945  $\text{cm}^{-1}$  from the C-H stretching of the methoxyl groups of the lignin is more pronounced, whereas in the  $S_2$  the peak at 2897  $\text{cm}^{-1}$ , attributed to C-H and C-H<sub>2</sub> stretching of the cellulose, dominates (Fig. 4c). The band at 1098  $\text{cm}^{-1}$  is assigned to asymmetric stretching vibration of C-O-C linkages of cellulose and is more pronounced in the  $S_2$  spectrum than in the CC spectrum (Fig. 4d).

### Raman Imaging of Cellulose Distribution

The cellulose distribution map was produced by integrating over the 2897  $\text{cm}^{-1}$  band, comprising the CH and CH<sub>2</sub> stretching vibration of cellulose (Gierlinger and Schwanninger 2006). Compared to lignin spatial distribution, cellulose distribution was much more uniform (Fig. 5).

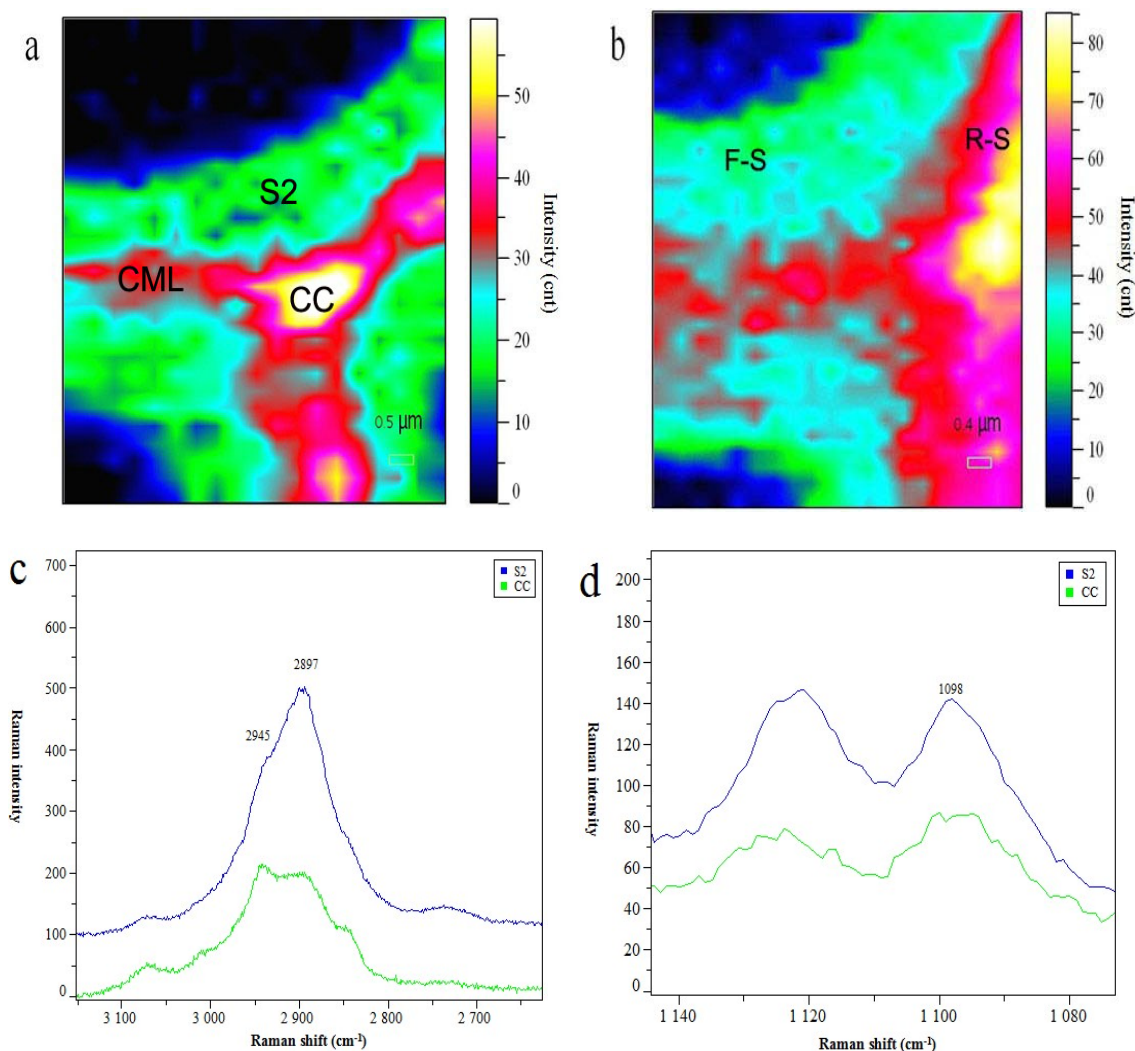


**Fig. 4.** Raman images showing the lignin distribution of fiber and ray parenchyma. (a) Lignin distribution in morphologically distinct regions of fiber, 1712-1519  $\text{cm}^{-1}$ ; (b) Lignin distribution in secondary wall of ray parenchyma, 1712-1519  $\text{cm}^{-1}$ , F-S: fiber secondary wall, R-S: ray secondary wall; (c) Zoom into the average Raman spectra acquired from the cell corner and the middle layer of fiber secondary wall, 3200-2625  $\text{cm}^{-1}$ ; (d) Zoom into the average Raman spectra acquired from the cell corner and the middle layer of fiber secondary wall, 1145-1070  $\text{cm}^{-1}$

Regions of highest lignin content, that is, CC, are known to be locations of low cellulose content (Meier 1985; Whiting and Goring 1983). High cellulose content (105-160 counts) spots were confined mostly to  $S_2$  and  $S_2$ - $S_3$  regions. For the  $S_2$  layer, cellulose distribution was much more uniform (mostly magenta/yellow) compared to that of lignin. Considering that cellulose is a crystalline polymer and is highly oriented (chain-axis largely perpendicular to the transverse section), it is likely that such intensity variation may be a reflection of the variation of cellulose content and orientation. The lumen  $S_3$  interface produced weak cellulose content and was the consequence of the fact that at such interfaces sampling included the contribution from the lumen. There are some areas of overlap where both cellulose and lignin are highly concentrated. For instance, some of the locations in the common area seem to be in the CML. Although, in the

present study we have assumed that the  $2897\text{ cm}^{-1}$  represents only cellulose, contributions from other polysaccharides cannot be ruled out. The complexity of wood's vibrational spectrum originates from its multicomponent nature, which was reflected by broad overlapping bands. Cellulose and hemicelluloses have similar chemical bonds and are therefore difficult to differentiate (Chu et al. 2010). Generally, the skeletal motions of most of the hemicelluloses result in fairly broad bands, unless they are so organized that they have a high degree of repetitive order.

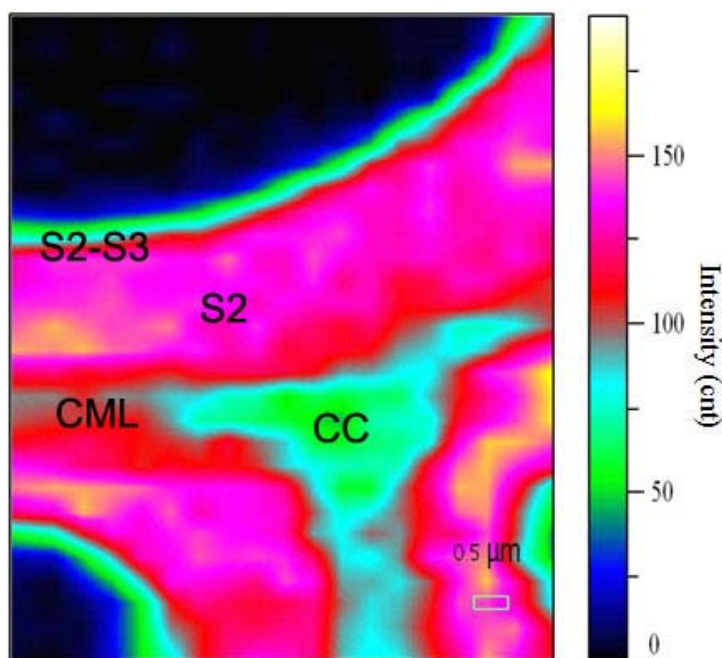


**Fig. 5.** Raman image showing the cellulose distribution of fiber,  $2950\text{-}2867\text{ cm}^{-1}$

The high degree of orientation of cellulose in the cell walls is also reflected in the spectra. The  $2897\text{ cm}^{-1}$  band due to the CH and  $\text{CH}_2$  stretching changes both in shape and in intensity when the plane of the cell wall relative to the polarization of the exciting radiation is adjusted. The changes in the  $1098\text{ cm}^{-1}$  skeletal band of cellulose are also consistent with the high degree of alignment of the cellulose. A zoom into the C-H, C-H<sub>2</sub> stretching region and into the C-O-C stretching region shows an even clearer change in the band height ratio of the average spectra of fiber S<sub>2</sub> and ray S<sub>2</sub>. In the S<sub>2</sub> of the ray cells, the band at  $2897\text{ cm}^{-1}$  is strongly reduced (Fig. 6a), the band at  $1098\text{ cm}^{-1}$  is increased (Fig. 6b). These observed changes in band height ratios are in context with the orientation of the cellulose molecule, as bands deriving from perpendicular oriented C-H bonds ( $2897\text{ cm}^{-1}$ ) decrease, while the parallel oriented C-O-C ( $1098\text{ cm}^{-1}$ ) increase (Gierlinger and Burgert 2006). These two band heights are highly sensitive to the orientation in cellulose. The observed variation in the band height ratios could be explained by the process of cell wall development and division. The cambium contains two morphological distinct cell types: axially elongated fusiform cambial cells (FCC), which develop into secondary xylem cells by periclinal division, and somewhat isodiametrical ray cambial cells (RCC), which develop into parenchyma cells by

anticlinal division (Mellerowicz et al. 2001). Thus, the ray parenchyma cell in our sample is in a plane parallel to the electric vector of the laser beam in y-directions, whereas the fiber is perpendicular. Accordingly, in the ray parenchyma  $S_2$  the intensity of perpendicular oriented C-H bonds decrease, while the parallel oriented C-O-C bonds increased.

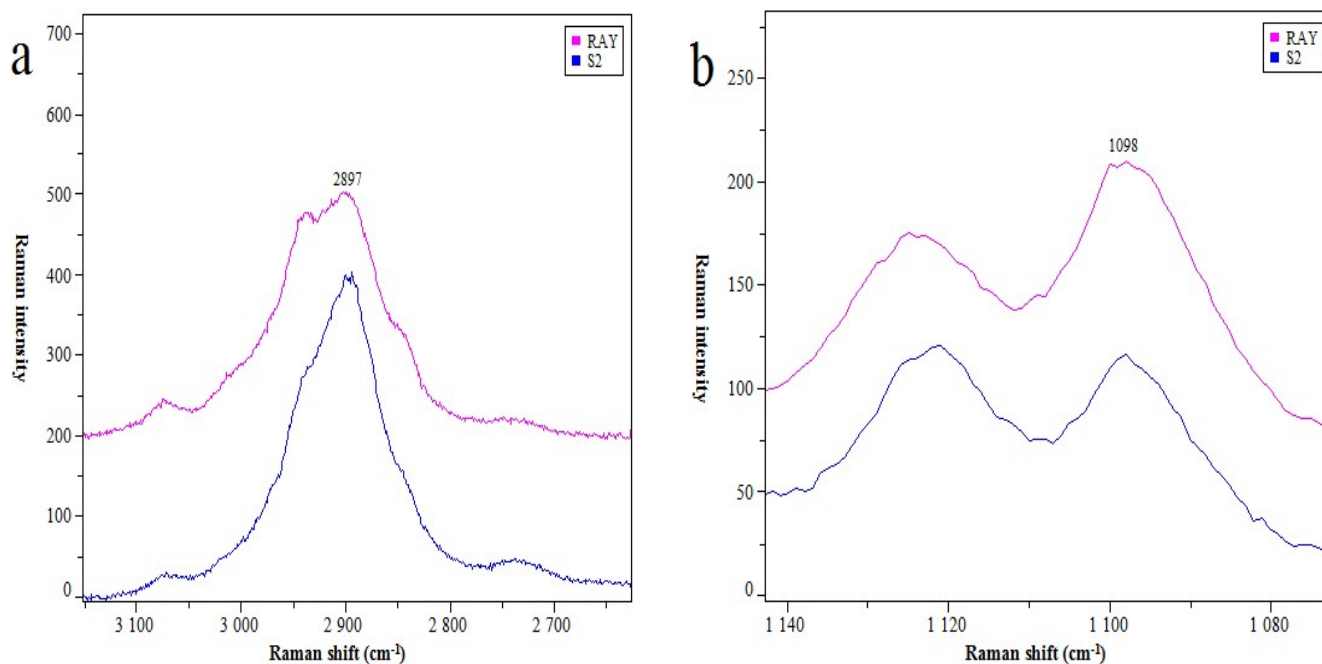


**Fig. 6.** (a) Zoom into the average Raman spectra acquired from the secondary wall of ray parenchyma and fiber, 3200-2625  $\text{cm}^{-1}$ ; (b) Zoom into the average Raman spectra acquired from the secondary wall of ray parenchyma and fiber, 1145-1070  $\text{cm}^{-1}$

## CONCLUSIONS

1. Raman images revealed that at the microscopic level the content of both lignin and cellulose differ between morphologically distinct regions. The CC lignin content was the highest on average, whereas the cellulose distribution, for the most part, showed the opposite pattern.
2. The change in the 2897  $\text{cm}^{-1}$  and 1098  $\text{cm}^{-1}$  band height ratio of ray parenchyma secondary wall indicated a high degree of orientation of cellulose.
3. SEM-EDXA results showed that lignin content ratio in CC, CML, and  $S_2$  is 1.4:1.1:1.
4. TEM images showed that fiber wall is divided into middle lamella (ML), primary wall (P), and secondary wall ( $S_1$ ,  $S_2$  and  $S_3$ ), and the staining intensities reveal differing lignin content.
5. The present results will contribute to fundamental understanding of the plant cell wall and provide information for the conversion of lignocellulosic biomass to biofuels.

## ACKNOWLEDGMENTS

This work was supported by the Grants from the Natural National Science Foundation of China (30871997 and 31070526), Major State Basic Research Projects of China (973-2010CB732204), Excellent Youth Foundation of Heilongjiang (JC200907), Programs in Graduate Science and Technology Innovation of Beijing Forestry University (BLYJ201110), and partially from China Ministry of Education (109020, NCET-08-0728), and State Forestry Administration (2009-4-16, 2010040706), China.

## REFERENCES CITED

- Åkerholm, M., and Salmén, L. (2003). "The oriented structure of lignin and its viscoelastic properties studied by static and dynamic FT-IR spectroscopy," *Holzforschung* 57(5), 459-465.
- Agarwal, U.P. (1999). "An overview of Raman spectroscopy as applied to lignocellulosic materials," In: Argyropoulos, E., (Ed.), *Advances in Lignocellulosics Characterization*, TAPPI Press, Atlanta, pp. 201-225.
- Agarwal, U.P. (2006). "Raman imaging to investigate ultrastructure and composition of plant cell walls: Distribution of lignin and cellulose in black spruce wood (*Picea mariana*)," *Planta* 224(5), 1141-1153.
- Agarwal, U. P., and Ralph, S. A. (1997). "FT-Raman spectroscopy of wood: Identifying contributions of lignin and carbohydrate polymers in the spectrum of black spruce," *Appl. Spectrosc.* 51(11), 1648-1650.
- Agarwal, U. P., and Ralph, S. A. (2008). "Determination of ethylenic residues in wood and TMP of spruce by FT-Raman spectroscopy," *Holzforschung* 62(6), 667-675.
- Abdul Khalil, H. P. S., Ireana Yusra, A. F., Bhat, A. H., and Jawaid, M. (2010). "Cell wall ultrastructure, anatomy, lignin distribution, and chemical composition of Malaysian cultivated kenaf fiber," *Ind. Crops. Prod.* 31(1), 113-121.
- Bland, D. E., Foster, R. C., and Logan, A. F. (1971). "The mechanism of permanganate and osmium tetroxide fixation and the distribution of the lignin in the cell wall of *Pinus radiata*," *Holzforschung* 25(5), 137-143.
- Boerjan, W., Ralph, J., and Baucher, M. (2003). "Lignin biosynthesis," *Annu. Rev. Plant Biol.* 54(1), 519-546.
- Cao, Y., Shen, D., Lu, Y.L., and Huang, Y. (2006). "A Raman-scattering study on the net orientation of biomacromolecules in the outer epidermal walls of mature wheat stems (*Triticum aestivum*)," *Ann. Bot.* 97(6), 1091-1094.
- Chu, L. Q., Masyuko, R., Sweedler, J. V., and Bohn, P. W. (2010). "Base-induced delignification of *miscanthus x giganteus* studied by three-dimensional confocal Raman imaging," *Bioresour. Technol.* 101(13), 4919-4925.
- Donaldson, L. A. (2001). "Lignification and lignin topochemistry-an ultrastructural view," *Phytochemistry* 57(6), 859-873.
- Donaldson, L. A., Hague, J., and Snell, R. (2001). "Lignin distribution in coppice poplar, linseed and wheat straw," *Holzforschung* 55(4), 379-385.

- Edwards, H. G. M., Farwell, D. W., and Webster, D. (1997). "FT-Raman microscopy of untreated natural plant fibres," *Spectrochim. Acta*, A 53(13), 2383-2392.
- Gierlinger, N., and Burgert, I. (2006). "Secondary cell wall polymers studied by confocal Raman microscopy: Spatial distribution, orientation, and molecular deformation," *N. Z. J. For Sci.* 36(1), 60-71.
- Gierlinger, N., and Schwanninger, M. (2006). "Chemical image of poplar wood cell walls by confocal Raman microscopy," *Plant Physiol.* 140(4), 1246-1254.
- Gierlinger, N., and Schwanninger, M. (2007). "The potential of Raman microscopy and Raman imaging in plant research," *Spectroscopy* 21(2), 69-89.
- Himmel, M. E., Ding, S. Y., Johnson, D. K., Adney, W. S., Nimlos, M. R., Brady, J. W., and Foust, T. D. (2007). "Biomass recalcitrance engineering plants and enzymes for biofuels production," *Science* 315(5813), 804-807.
- Kataoka, Y., Saiki, H., and Fujita, M. (1992). "Arrangement and superimposition of cellulose microfibrils in the secondary walls of coniferous tracheids," *Mokuzai Gakkaishi* 38(4), 327-335.
- Kurti, E., Heyd, D. V., and Stephen, W. R. (2005). "Raman microscopy for the quantitation of propiconazole in white spruce," *Wood. Sci. Technol.* 39(8), 618-629.
- Maurer, A., and Fengel, D. (1991). "Electron microscopic representation of structural details in softwood cell walls by very thin ultramicrotome sections," *Holz Roh Werkst.* 49, 53-56.
- Meier, H. (1985). "Localization of polysaccharides in wood cell walls," In: Higuchi, T., (ed.), *Biosynthesis and Biodegradation of Wood Components*, Academic Press, Orlando, Florida, pp. 43-50.
- Mellerowicz, E. J., Baucher, M., Sundberg, B., and Boerjan, W. (2001). "Unravelling cell wall formation in the woody dicot stem," *Plant Mol. Biol.* 47(1-2), 239-274.
- Rösch, P., Schneider, H., Zimmermann, U., Kiefer, W., and Popp, J. (2004). "In situ Raman investigation of single lipid droplets in the water-conducting xylem of four woody plant species," *Biopolymers* 74(1-2), 151-156.
- Rubin, E. M. (2008). "Genomics of cellulosic biofuels," *Nature* 454, 841-845.
- Saka, S. (1982). "Evaluation of the quantitative assay of lignin distribution by SEM-EDXA technique," *Wood. Sci. Technol.* 16(1), 1-18.
- Saar, B. G., Zeng, Y., Freudiger, C. W., Liu, Y. S., Himmel, M. E., Xie, X. S., and Ding, S. Y. (2010). "Label-free, real-time monitoring of biomass processing with simulated Raman scattering microscopy," *Angew. Chem. Int. Ed.* 49, 5476-5479.
- Saariaho, A. M., Jääskläinen, A. S., Nuopponen, M., and Vourinen, T. (2003). "Ultra violet resonance Raman spectroscopy in lignin analysis: Determination of characteristic vibrations of p-hydroxyphenyl, guaiacyl, and syringyl lignin structures," *Appl. Spectrosc.* 57(1), 58-66.
- Schmidt, M., Schwartzberg, A. M., Perera, P. N., Weber-Bargioni, A., Carroll, A., Sarkar, P., Bosneaga, E., Urban, J. J., Song, J., Balakshin, M. Y., Capanema, E. A., Auer, M., Adams, P. D., Chiang, V. L., and James Schuck, P. (2009). "Label-free in situ imaging of lignification in the cell wall of low lignin transgenic *Populus trichocarpa*," *Planta* 230(3), 589-597.

- Schmidt, M., Schwartzberg, A. M., Carroll, A., Chaibang, A., Adams, P. D., and Schuck, P. J. (2010). "Raman imaging of cell wall polymers in *Arabidopsis thaliana*," *Biochem. Biophys. Res. Commun.* 395(4), 521-523.
- Singh, A., and Daniel, G. (2001). "The S2 layer in the tracheid walls of *Picea abies* wood: Inhomogeneity in lignin distribution and cell wall microstructure," *Holzforschung* 55(4), 373-378.
- Singh, A., Daniel, G., and Nilsson, T. (2002). "Ultrastructure of the S2 layer in relation to lignin distribution in *Pinus radiata* tracheids," *J. Wood Sci.* 48(2), 95-98.
- Takabe, K., Fujita, M., Harada, H., and Saiki, H. (1986). "Lignification process in *Cryptomeria* (*Cryptomeria japonica* D. Don) tracheid: Electron microscopic observation of lignin skeleton of differentiating xylem," *Res. Bull. Coll. Exp. For. Hokkaido Univ.* 43, 783-788.
- Terashima, N. (2000). "Formation and ultrastructure of lignified plant cell walls," In: Kim, Y. S., (ed.), *New Horizons in Wood Anatomy*, Chonnam National University Press, Gwangju, Korea, pp. 169-180.
- Whiting, P., and Goring, D. A. I. (1983). "The composition of carbohydrates in the middle lamella and secondary wall of tracheids from black spruce wood," *Can. J. Chem.* 61, 506-508.
- Wiley, J. H., and Atalla, R. H. (1987). "Band assignment in the Raman spectra of celluloses," *Carbohydr. Res.* 160, 113-129.
- Xu, F., Zhong, X. C., Sun, R. C., and Lu, Q. (2006). "Anatomy, ultrastructure and lignin distribution in cell wall of *Caragana Korshinskii*," *Ind. Crops. Prod.* 24(2), 186-193.
- Yoshinaga, A., Fujita, M., and Saiki, H. (1992). "Relationships between cell evolution and lignin structural varieties in oak xylem evaluated by microscopic spectrophotometry with separated cell walls," *Mokuzai Gakkaishi* 38(7), 629-637.

Article submitted: June 29, 2011; Peer review completed: July 28, 2011; Revised version received and accepted: August 13, 2011; Published: August 14, 2011.